Study of single nanoparticle spectroscopy and Exciton-plasmon coupling

A Thesis

submitted to
Indian Institute of Science Education and Research Pune
in partial fulfillment of the requirements for the
BS-MS Dual Degree Programme

by

Rajath R Sawant
20121035

Indian Institute of Science Education and Research Pune
Dr. Homi Bhabha Road,
Pashan, Pune 411008, INDIA.

April, 2017

Supervisor: Dr.G V Pavan Kumar

Certificate

This is to certify that this dissertation entitled Study of single nanoparticle spectroscopy and Exciton-plasmon coupling towards the partial fulfilment of the BS-MS dual degree programme at the Indian Institute of Science Education and Research, Pune represents study/work carried out by Rajath R Sawant at Indian Institute of Science Education and

Research under the supervision of Dr.G V Pavan Kumar, Assistant Professor, Department of Physics , during the academic year 2016-2017.

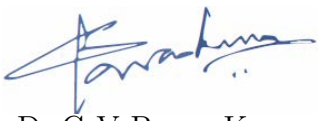

Dr.G V Pavan Kumar

Rajath R Sawant

Committee:

Dr.G V Pavan Kumar

Dr.Nirmalya Ballav

This thesis is dedicated to my parents

Declaration

I hereby declare that the matter embodied in the report entitled Study of single nanoparticle spectroscopy and Exciton-plasmon coupling are the results of the work carried out by me at the Department of Physics, Indian Institute of Science Education and Research, Pune under the supervision of Dr.G V Pavan Kumar and the same has not been submitted elsewhere for any other degree.

Dr.G V Pavan Kumar

Rajath R Sawant

Acknowledgements

Foremost, I would like to thank my guide Dr.G V Pavan Kumar for his guidance and constant support. He has always given me freedom to think in different ways, at the same time correcting me whenever I was wrong. I am grateful to him for believing in me and encouraging me to move forward, overlooking my faults.

Special thanks to Adarsh Vasista, whose advice I have always sought regarding my research. I would also like to thank him for building the Fourier plane imaging and spectroscopy setup which has been of great utility to my 5^{th} year work. The fruitful discussions I had with him, be it regarding Physics, literature or politics, has greatly helped me. I would like to extend my thanks to the former Postdoctoral fellow in our group Dr.Debrina Jana for her assistance in synthesis work and her useful advice. Many thanks to the other doctoral students in the group Danveer Singh for the preparation of silver nanowires and Ravi Tripathi for Scanning Electron Microscopy imaging of my samples. I would also like to thank our collaborators at IIT-Bombay for providing me with samples on which my MS research was carried out.

All my lab members, Harshvardhan Jog, Jesil Jose, Deepak Kumar Sharma, Vandana Sharma, Shailendra Chaubey, Sunny Tiwari, Diptabrata Paul have been a great support to me in my research. I would always cherish the discussions that we had during chai-time, both academic and non-academic. Thanks to the people in H-cross for helping me carry out various studies.

Many thanks to all of my friends for their generous support and encouragement. Finally, I express my deep gratitude to my family for being with me. Their support was invaluable.

Abstract

Plasmonic nanostructures give major insights into the interaction between light and matter at nanoscale. Also, they have potential practical applications in various fields such as in biosensing(sensing of different types of molecules, proteins), plasmonic circuits, as metamaterials. The realization of their practical application is possible only when one understands their properties entirely. Therefore, in this thesis, we study the technique to understand localized surface plasmon resonance(LSPR) properties. Also, we have made an attempt to probe the plasmon-exciton coupling. Therefore this thesis is divided into two parts.

In the first part, we have studied a technique which can collect single particle spectra called dark field spectroscopy. The setup is based on Total Internal Reflection of light. The study is majorly focused on scattering due to sub-wavelength structures. Gold nanostars prepared by us was probed by dark field scattering technique. We have discussed the information that we can extract from the spectra obtained.

The next part is focused on coupling of plasmonic nanostructure with two-dimensional material Molybdenum disulfide MoS_2 which is an excitonic material. 2-D material MoS_2 has tremendous applications in the field of optoelectronics because of their direct bandgap nature because of which it shows Photoluminescence. Our system comprises of silver nanowires on few layers of MoS_2. In our experiments, we have compared the Photoluminescence emission from MoS_2 and that from wire on MoS_2, both its magnitude and directionality. Our results show that silver nanowire on MoS_2 shows nanoantenna effect. Taking this study forward can give major insights about coupling of excitons and plasmons, also the results themselves have implications in nanophotonic circuits.

Contents

List of Figures

Chapter 1

Introduction

1.1 LSPR

Metals are composed of delocalized free electrons. The quantum of collective oscillation of these electrons is called a Plasmon. It is nothing but the motion of electron gas with respect to the positive ion core under the influence of external electric field. The frequency of plasma oscillations is given by:

$$\omega_p = \sqrt{\frac{ne^2}{m\epsilon_0}}$$

When light is incident on metals, photons get coupled with surface plasmons and surface waves are set in motion. These quasiparticles are known as Surface Plasmon Polaritons (SPP). These surface waves occur at the interface only when the real part of dielectric permittivity (ϵ) of one region is positive and another is negative. For noble metals, the real part of ϵ is negative in visible region.

The mathematical picture of this coupling can be obtained by solving Maxwell's equation for dielectric and metal regions(Appendix).

When the surface plasmons are confined in sub-wavelength structures (below the wavelength of incident light), they are said to be localized surface plasmons. Electric field is greatly enhanced in the vicinity of surface of particles in this case and rapidly attenuates

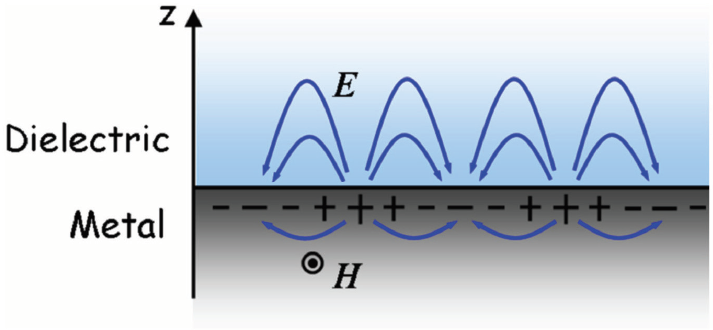

Figure 1.1: A Surface Plamon Polariton propagating along metal dielectric interface [1]

when one moves away from the surface. The optical extinction (Absorption + scattering) peaks at a particular wavelength for a particle called as Localized Surface Plasmon Resonance (LSPR). The LSPR is a function of particle's composition, size, shape and refractive index of surrounding environment.

1.2 Scattering theory

Mie scattering theory explains the scattering due to particles of size comparable to the wavelength of incident light. This theory also encompasses Rayleigh scattering when minute particle limit is applied [8]. Assuming Rayleigh scattering, the scattering cross-section of a spherical particle of volume V is given by

$$\sigma_{sca} = \frac{32\pi^4\epsilon_m^2 V^2}{\lambda^4}\frac{(\epsilon_1-\epsilon_m)^2+\epsilon_2^2}{(\epsilon_1+2\epsilon_m)^2+\epsilon_2^2}$$

$$\sigma_{ext} = \frac{18\pi\epsilon_m^{\frac{3}{2}} V}{\lambda}\frac{\epsilon_2}{(\epsilon_1+2\epsilon_m)^2+\epsilon_2^2}$$

$$\text{where } \sigma_{ext} = \sigma_{abs} + \sigma_{sca}$$

where the dielectric constant of metal $\epsilon = \epsilon_1 + i\epsilon_2, \epsilon_m$ is the dielectric constant of the surrounding medium,λ is the wavelength of incident light.

We can see from the expression for scattering cross section that it varies as square of the volume. As a result of this, the scattering process dominates for larger particles. Also σ_{sca} is maximized when $\epsilon_1 + 2\epsilon_m$ goes to zero. Hence the wavelength at which this condition is satisfied gives the peak position in LSPR. This also explains the surrounding dielectric environment dependence of LSPR. The expression for extinction cross section resembles the functional form of a Lorentzian. Comparing the terms of a Lorentzian function with this expression shows that full width at half maximum (FWHM) of the plasmon resonance is proportional to ϵ_2 [9]. Hence the imaginary part of the dielectric function is related to damping, that is resonance peak broadening. Rayleigh scattering can also be derived from Mie scattering theory. Rayleigh scattering is valid only for particles whose radius is less than one-tenth of incident light wavelength [8]. One major difference in these two cases is that Rayleigh scattering is uniform in all directions but for Mie scattering forward scattering is more compared to backward scattering.

The plasmon resonance line width and position depends on the size and shape of the particle and also refractive index of the surrounding medium. From extinction cross section expression, it can be deduced that ϵ_m contributes to both the FWHM of plasmon resonance as well as the position of the resonance peak. Higher the refractive index of the medium, more is the resonance red-shift. Hence by following the resonance peak, one can sense the change in the refractive index of surrounding medium. This has huge biomedical applications. One limitation of the LSPR sensors is that they lose their sensitivity in the range of 5 to 30 nm from the medium.

The LSPR peak position is not very sensitive to the size of the particle. For particles whose radius is much smaller than 100 nm, only dipolar term contributes. This is called dipolar approximation. This is also referred to as quasi-static approximation as electric field is considered to be constant throughout the surface of the particle. It is a very important assumption because the interaction of a particle with incident light can be dealt with electrostatics. In this limit, the main contribution to extinction is from absorption, as dipolar scattering varies as $(\frac{R}{\lambda})^6$ which is very small. For larger particles whose radius is comparable to the wavelength of incident light, the quasistatic approximation is no longer valid as along with dipolar terms, quadrupolar and higher terms also contribute to the extinction. Also scattering dominates over absorption unlike in the previous case. In the process of scattering, light excites plasmons in the nanoparticles which can decay in radiative and non-radiative manner. Since energy is lost, radiative decay causes damping. Hence larger sized particles

have higher line width because of damping due to scattering and phase retardation.

1.3 Dark field spectroscopy

In conventional spectroscopy, the spectra of an ensemble of particles is collected. Unlike this, dark field spectroscopy enables one to collect spectra from single particles. This is a very useful technique as one can associate spectra of a particle to its size and shape by performing correlation studies [10]. As mentioned in the previous section, a plethora of information can be obtained from single particle spectra about the particle as well as its surrounding [11].

What is a dark field image? It is nothing but the collection of only the scattered light from particles and eliminating the background light unlike in a bright field image. Single metal nanoparticles are seen as colorful points in dark background. Hence it is a valuable tool to do single particle spectroscopy. There are many ways to achieve dark field setup. The most popular one is using dark field condenser. It is usually carried out in transmission geometry with a white light source. The condenser is a lens which has high numerical aperture and allows light to be incident only at higher angles on the sample. The objective lens which collects scattered light from the top side has a numerical aperture smaller than that of the condenser lens. This condition has to be satisfied as the background light is to be eliminated to obtain a dark field image.

But we employed a different geometry to achieve dark field microscopy. The setup and technique is explained in the next section.

1.4 Excitonics

1.4.1 2-D materials

The materials which are only a few atomic layers thick are called 2-D materials. They behave differently as compared to the bulk form of the same material. The charge carriers are confined to move only in a plane which gives rise to interesting mechanical and optical properties. For instance, Graphene which is the 2-D form of Graphite is known to have highest

thermal and electrical conductivity. They interact strongly with light which makes them a favourable candidate for optoelectronic devices. Parallel to graphene, semiconductor 2-D materials are also of interest when it comes to device fabrication. Most popular among them are Transition Metal DiChalcogenides (TMDC); One major reason for their applicability is their bandgap which falls in near infrared-visible region unlike graphene, which behaves as a conductor. Layered Transition Metal DiChalcogenides give rise to new physical phenomena because of d-electron interaction. Molybdenum disulphide (MoS_2) is one of the members of TMDC family and we have focused our study on this.

MoS_2 is made of covalently bonded S-Mo-S sheets. Each sheet is bound to another by weak van der Waals forces. Because of relatively weak force between the layers and strong intralayer interaction, formation of ultrathin layer by mechanical exfoliation is possible.

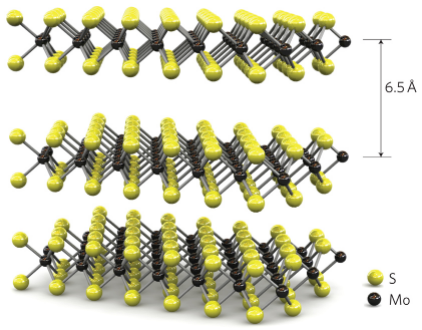

Figure 1.2: Structure of MoS_2 single layers [2]

MoS_2 in its bulk form is an indirect band gap material with a band gap of about 1 eV [12]. But as the layers reduce the band gap turns from indirect to direct. Monolayer MoS_2 is a perfectly direct band gap material with a band gap of 1.8 eV. In direct bandgap, the top of valence band and bottom of conduction band are at the same value of crystal momentum whereas for an indirect bandgap they occur at different values of momentum in the Brilluion zone. It is about 0.7 nm thick which can be measured using by Atomic Force Microscope (AFM). The nature of band gap has implications for light absorption and radiative recombination. This affects the amount of emission which shows up in Photoluminescence intensity.

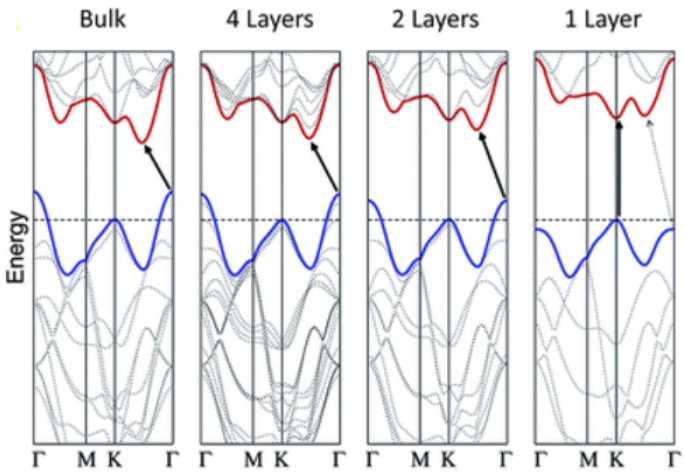

Figure 1.3: Band diagram calculated using Density functional theory for bulk MoS_2, quadrilayer MoS_2, bilayer MoS_2, monolayer MoS_2 [3] [4]

1.4.2 Excitons

Exciton is an electron-hole pair quasiparticle formed due to electronic excitation. It can be treated as electrically neutral particle capable of diffusion. Hence they transport energy across the material without transporting electric charge. There are mainly 2 types of excitons, Wannier excitons and Frenkel excitons. Wannier excitons typically occur in materials with a large dielectric constant which is generally the case in semiconductors. As a result of this, Coulombic interaction between electron and hole is screened. This leads to larger radius for Wannier excitons, which is larger than the lattice spacing. Frenkel excitons are formed in materials with low dielectric constant, hence their radius is small.

Excitons in MoS_2

An exciton is formed in a semiconductor when a photon is absorbed by it. This excites an electron from valence band to conduction band. This leaves behind a positively charged 'hole' in valence band. Monolayer MoS_2 shows two kinds of excitons, A and B excitons. This is because the highest valence band at K point in the band structure of MoS_2 splits by around 150 meV because of large spin-orbit interaction [13]. The excitation from two different points at K point to the bottom of conduction band gives rise to two different

excitons. The Photoluminescence peaks at 1.88 eV($\approx$ 660 nm) and 2.02 eV($\approx$ 613 nm) of monolayer MoS_2 can be attributed to A and B excitons respectively. In few layers and bulk MoS_2, this splitting is due to both spin-orbit interaction and interlayer interaction. Also, in this case along with direct bandgap transition, an exciton due to indirect bandgap transition(1.29 eV) is also seen [14].

1.4.3 Photoluminescence

When a semiconductor is hit with photons whose energy is greater than bandgap energy, it gets excited. Once the photons are absorbed, electrons are transferred to conduction band and holes are formed in valence band forming excitons. The excitation undergoes relaxation by recombination of electrons and holes resulting in the emission of light. This process of excitation using light resulting in the spontaneous emission of radiation from the material is called Photoluminescence.

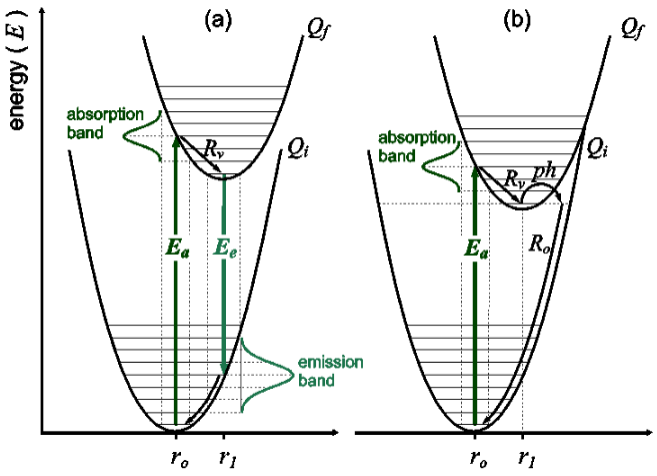

Figure 1.4: Excitation, emission, relaxation explained using configuration coordinate diagram for a)radiative transition b)non-radiative transition [5]

In the figure 1.4, an offset is assumed between ground state and excited state. Upon excitation, electrons are excited from ground state to a higher vibrational state in the excited electronic state in a broad optical band as shown in figure 1.4 a). This is followed by relaxation of electrons to the lowest vibrational state by emitting extra energy to the surroundings which usually occurs by a phonon-mediated nonradiative process. From lowest

vibrational state electrons relaxes to ground state by emitting photons [15]. The absorption and emission band peak and their linewidth is also shown. In 1.4 b), non-radiative transition of an electron is shown. The luminescence quantum efficiency is given by number of photons emitted divided by the number of photons absorbed.

Chapter 2

Synthesis of gold nanostars

As described in the previous section, plasmonic particles show many interesting optical properties as they strongly absorb and scatter light by a phenomenon called Localized Surface Plasmon Resonance (LSPR). By modifying the shape and morphology of these structures one has control over their behaviour. Hence by tuning their size and shape, they can be prepared as required for a specific application.

For my project, I have focused on gold nanostars as they were required for single particle studies. Nanostars are defined as a nanostructure with a central core with several protruding arms with sharp tips branching from it. One striking feature of this structure is that the local field strength in the vicinity of tips is enhanced by several orders of magnitude when compared to the incident light [16]. Gold nanostars were synthesized by us by a 2 step process. It is a seed mediated process in which icosahedral seeds are grown in the first step and the sharp tips are grown on the facets symmetrically in the next step [17].

The procedure for the synthesis is as follows. 0.1 grams of Poly Vinyl Pyrrolidone (PVP) was dissolved in 25 millilitres of Diethylene Glycol (DEG)in a round bottomed flask and heated until it was refluxed. After few minutes, 2 ml solution of Diethylene Glycol (DEG)containing 20 milligrams of $HAuCl_4.3H_2O$ was inserted into the above the solution. The reaction was stopped after 10 minutes and was allowed to cool. Later it was centrifuged and washed several times with Dimethyl Formamide (DMF). The icosahedral seeds obtained is dispersed in 27 ml of Dimethyl Formamide (DMF)and was stored for characterization. For the second step, in 15 ml of Dimethyl Formamide (DMF), 1.2 grams of Poly Vinyl Pyrroli-

done (PVP)was dissolved. To this solution, 80 microlitres of 2.5 M of Hydrochloric acid and 50 microlitres of 40% Dimethyl Acetamide (DMA) was added to the solution. 1 millilitre of icosahedral seeds prepared in the previous step was added to the solution. Subsequently, 20 microlitres of 0.5 M $HAuCl_4$ solution was added to this. This reaction solution was stirred and heated using oil bath at 80^o C for around four hours. Centrifugation and washing of the product were done with ethanol. The obtained nanostars were finally dispersed in 2 millilitres of water.

The characterization of the nanostructures obtained is as follows. Figure 2.1 is the image of an icosahedral seed after step one. When viewed from one direction, five triangular faces are visible which is typical of an icosahedron.

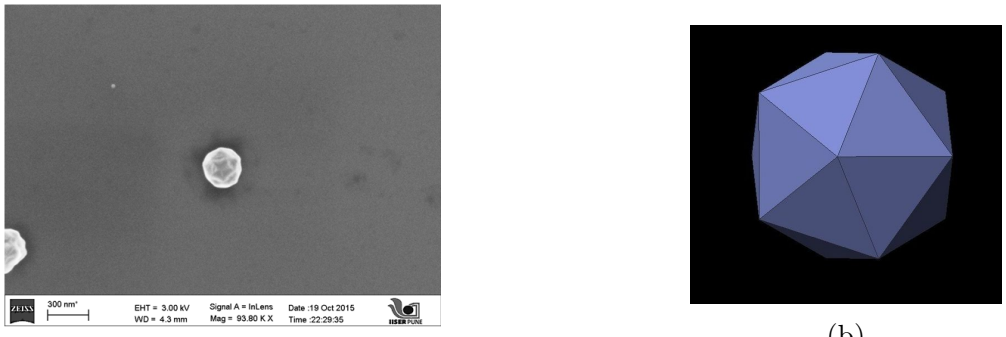

(a) (b)

Figure 2.1: A)FESEM image of a icosahedral seed B)A 3-D figure of a regular icosahedron

From the figure 2.2, it is evident that the size of the seed is around 150-200 nm. The amount of Dimethyl Acetamide (DMA)in the subsequent step dictates the sharpness of the arms of stars to be formed. Along with this, appropriate amount of Hydrochloric acid will ensure the growth of hexagonal bipyramidal arms on specific facets ensuring the formation of stars like structures.

The gold nanostars were not highly monodispersed. Their average size was around 250 to 300 nm. To indeed confirm that the geometry of stars is different than that of seeds, we collected UV-Visible absorption spectra of both the entities. The changes in spectra can be used as a confirmation for change in the structure (Figure 2.3).

The spectra peak positions roughly matches with that given in the paper referred [17]. Two peaks have merged in the spectrum of nanostars. Dark field spectra measurements were

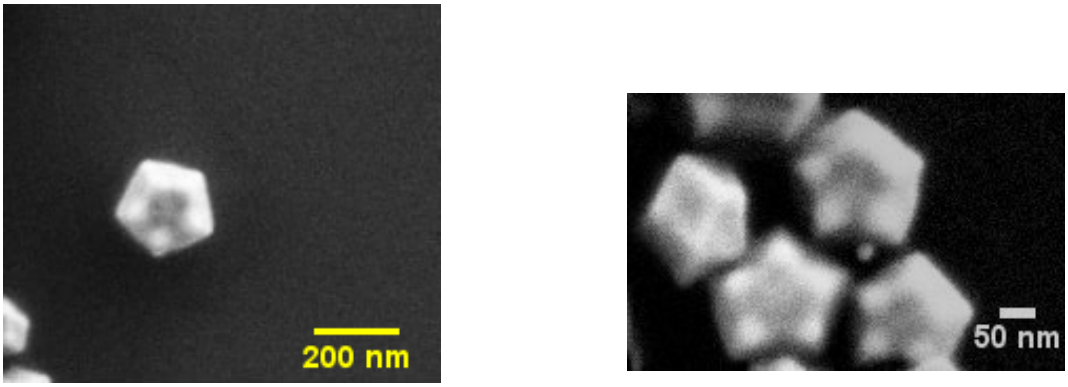

(a) (b)

Figure 2.2: FESEM images of gold nanostars

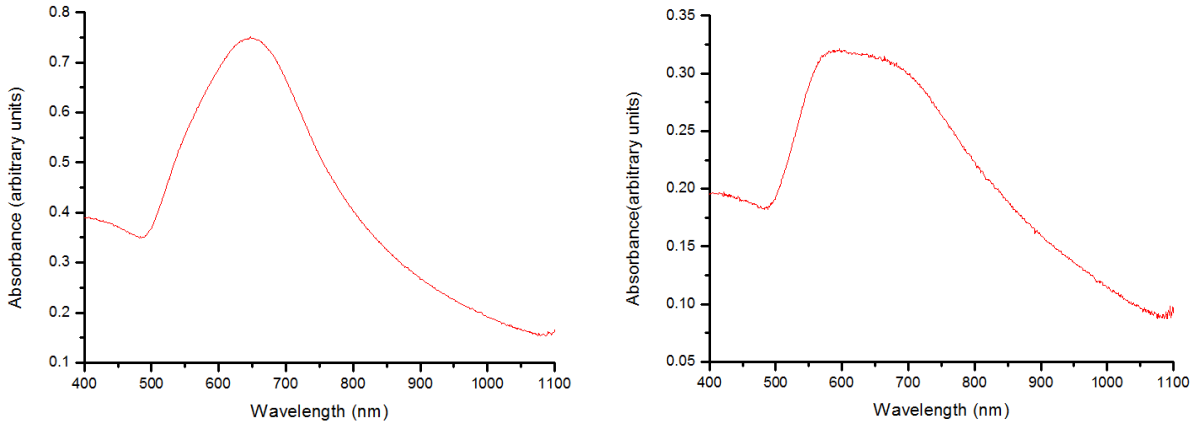

(a) (b)

Figure 2.3: Absorption spectra of a)Icosahedral seeds b)Gold nanostars

done on these structures which is discussed in the next section.

Chapter 3

Dark field spectroscopy

3.1 Motivation

As discussed in the introductory section, dark field spectroscopy has far-reaching applications in the field of Plasmonics. It is an important characterization tool if one wants to perform single particle studies. Single particle studies have advantages over ensemble measurements in many aspects. Synthesis of nanoparticles always produce particles of distribution of shapes and sizes. This inhomogeneity causes broadening of extinction spectra of an ensemble. Hence to say anything specific about particles, single particle spectra is necessary. Not just the particle but its local environment can be probed by this technique [8]. Along with individual particles, a combination of particles like dumbells formed from two spherical particles or pair of nanorods can be probed which is clearly not possible to extract from an ensemble. The hotspots in their junction is an important aspect to study. Targeted action can be applied to single particles, for instance changing the position of a trapped single nanoparticle.

Conventional optical microscopes can be used to study large objects like cells and tissues in detail but they are diffraction limited. Diffraction limit is approximated to be $\frac{\lambda}{2}$ where λ is the wavelength of incident light. Hence any specimen around 300nm and below is hard to study using an optical microscope. Various other single particle microscopy techniques are possible such as Electron microscopy, Scanning tunnelling microscopy which are near-field techniques. They require much sophisticated instruments to do the job. A more simpler setup is possible called dark field spectroscopy which is based on resonant light scattering

of plasmonic nanoparticles. It overcomes the shortcoming of optical microscope that it is not diffraction limited and can probe sub-wavelength scale particles. Moreover, it is based on Localized Surface Plasmon Resonance (LSPR) through which processes like field enhancement, nonlinear scattering, light trapping can be studied in greater detail. Also its possible applications in the development of biosensors, solar cells etc makes it an attractive technique to look into.

Our aim was to construct a setup which could illuminate particles, collect scattered light from the particles and route it to the spectrometer. The processing of obtained spectra had to be done to draw a meaningful conclusion about the particles under study.

3.2 Dark field spectroscopy setup

3.2.1 Apparatus

To achieve dark field microscopy, we have employed Total Internal Reflection (TIR) based illumination of nanoparticles instead of the well-known condenser based microscopy. For illumination, a supercontinuum light source is used. Nanoparticles sample is placed on a coverslip and is allowed to dry. This is placed on a dove prism using oil in the gap to match the refractive index of coverslip and prism (Figure 3.1). This aids in optically coupling them.

The light from supercontinuum source is let into dove prism through one of its faces as shown in figure 3.1. The angle of incidence is such that this ray gets total internally reflected at the face where the sample is placed. The evanescent waves produced at the interface illuminates the plasmonic particles. Hence this a near-field illumination [18]. Only nanoparticles which respond to these waves scatter light. Hence particles glow in the dark background. The scattered light is collected in the far-field by an objective lens of magnification 100X. The numerical aperture is 0.95 in some cases and 0.8 NA in some other. The collected light from objective lens is routed to Charged Coupled Device(CCD) camera to capture dark field images and to a spectrometer to collect spectra. Beam splitter in the path splits the light into two paths. The objective lens, camera and spectrometer are a part of industry built LabRam HR setup. setup. It is a confocal setup, meaning it collects signal from only a small region in the object plane. The confocal slit placed before the spectrometer does this job of

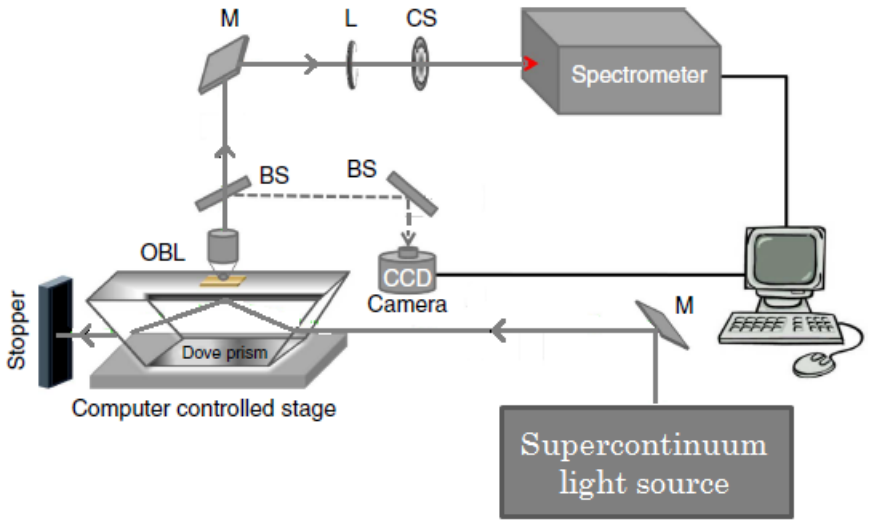

Figure 3.1: Dark field microscopy and spectroscopy setup. BS: Beam Splitter, M: Mirror, CS: Confocal slit, OBL: Objective lens, L: Lens

spatial selection. The stage on which prism is placed is computer controlled for positioning of the sample.

The sample is first imaged by CCD and an area is selected where there are less amount of scatterers so that there is less amount of background in the signal to be collected. The particle of interest is placed at the centre of the screen where there is a mark. The CCD camera path is cutoff by removing the beam splitter and all the light is sent directly to the spectrometer. We studied gold nanostars synthesized by us which is described in the previous chapter.

3.2.2 Results

From the Figure 3.2 it is evident that higher NA objectives are convenient for collecting spectra as the background signal is significantly reduced and Signal to Noise ratio is improved compared to lower NA objective. Therefore we used 0.95 NA, 100X objective for our further studies.

We selected a scatterer which is faint and small in size since possibility of it being a

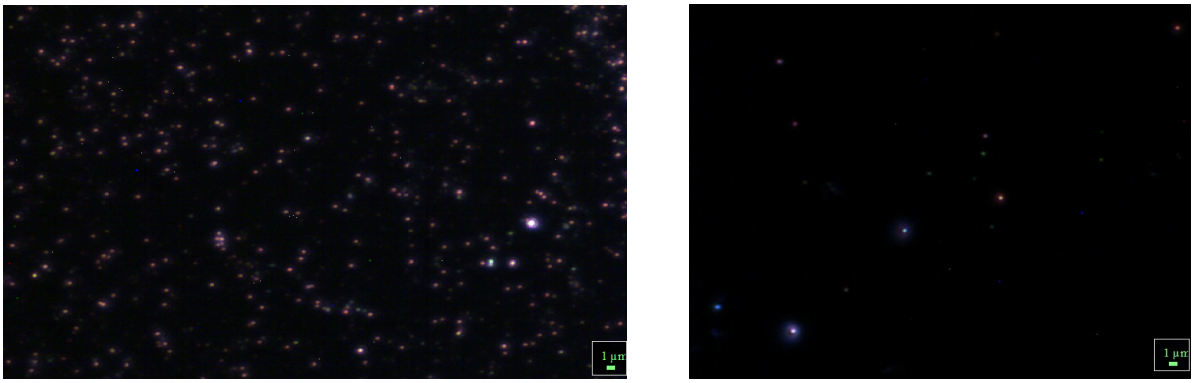

Figure 3.2: Dark field image of Gold nanostars captured with 100X of different samples a)0.8 NA objective b)0.95 NA objective

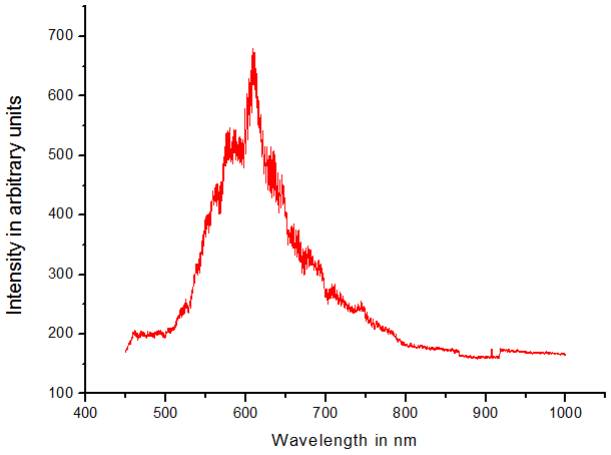

Figure 3.3: Raw Dark field spectrum of gold nanostars

single nanoparticle is high. The spectrum from such a point was collected (Figure 3.3). The signal was smoothened out using adjacent-averaging method. But the obtained signal was just a raw spectrum. It had to be processed further to get a final dark field signal. This was got by eliminating background noise from the data and normalizing it with the spectra of light source. Normalization is necessary because the spectra of supercontinuum source is not uniform in the whole range of wavelength being studied. Therefore the processing was done according to the following relation.

$$E_{final} = \frac{E_{raw} - E_{bkg}}{E_{light} - E_{dark}}$$

E_{bkg} is the signal collected from any point in the vicinity of particle under study where there are no scatterers. E_{light} is the spectra of diffused light from supercontinuum light source. E_{dark} is the spectra collected by switching off all light sources. This is to eliminate any electronic stray signal in the spectrometer. The final spectrum after processing is as shown in Figure 3.4 in which a clear picture emerges.

The final dark field spectrum is also smoothened out by adjacent-averaging method. In this method, a particular number of adjacent points (m) are considered. The values at these points are replaced by their average value. In our case m=5 is set. This method is employed when there is white noise in the spectrum which is the case in the following plot.

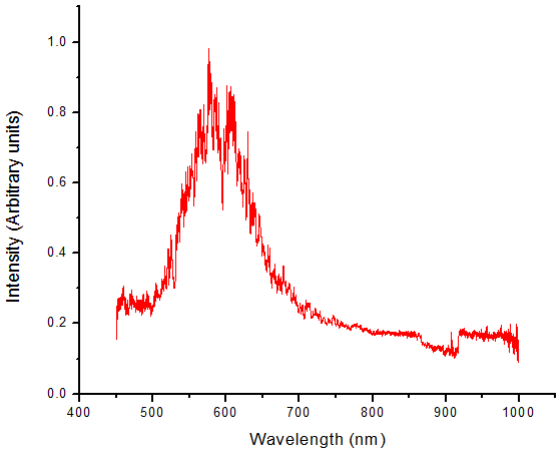

Figure 3.4: Final Dark field spectrum of gold nanostars

Looking at the spectrum, one can say that there are two peaks merged. Interestingly, we also see this feature in UV-Visible spectrum of an ensemble of nanostars but the dark field spectra being sharper than the ensemble spectra. This is on expected lines as discussed before.

3.2.3 Discussion

To infer anything about the particle and to confirm it is indeed a single particle, one is looking at, doing a correlation measurement is necessary [19]. By marking the substrate with focused ion beam lithography, the areas on the sample can be collocated in optical and electron microscopes. By first doing a Scanning Electron Microscopy (SEM) imaging, one

can note the addresses of single particles and clusters of particles can be discarded. Collecting spectra from identified locations gives the single particle spectra. Indirect methods such as comparing spectrum with already known spectrum of particles of a particular geometry can also be employed. Statistical methods are also known in which spectra from many scatterers are collected. By plotting them as frequency versus peak intensity, one can infer which of these scatterers are single particles [19]. But these methods are applicable only in certain conditions and have their own limitations. They are not as rigorous as correlation study.

As discussed in the introduction, position of LSPR peak and plasmon linewidth are the important information we obtain from dark field spectra.

Chapter 4

Silver nanowires on few layers of MoS_2

4.1 Motivation

Two-dimensional MoS_2 nanosheet is a potential candidate for ultrathin, transparent and flexible optoelectronic devices [20] as discussed in the introduction, as it has a bandgap and exhibits Photoluminescence (PL). As the number of layers of MoS_2 decreases, its PL emission efficiency increases [21]. However, the relatively lower light emission is one main bottleneck. The quantum yield of emission of monolayer MoS_2 is of the order of 10^{-3}. Hence there is a great need for enhancement of excitonic emission if they are to be realized for application as light emitters. It has been shown that this can be done by manipulating dielectric environment of MoS_2. One way is to couple plasmonic structures with MoS_2. The surface plasmon oscillations generated in subwavelength nanostructures causes local field enhancement in its vicinity and hence manipulate excitonic emission. This has been already shown with silver nanowires, gold nanorods, silver nanodisks.

The hybrid structure of silver nanowires on few layers of MoS_2 is what we chose to study. Silver nanowires act as both receiving and emitting antenna which is called nanoantenna effect [22]. We wanted to probe the magnitude and directionality of excitonic emission of MoS_2 in the presence of silver nanowires in the anticipation of nanoantenna effect. Moreover, the propagation of Surface Plasmon Polaritons in nanowires can act as a plasmonic waveguide. Studying the propagated light through nanowires in the presence of MoS_2 would be interesting. This aspect would have huge implications in optoelectronics. Partially overlapping

silver nanowires on a monolayer MoS_2 flake has been shown to act as an excitonic transistor in nanophotonic circuits. [23]

4.2 Experimental setup

The MoS_2 sample used for the experiments were grown by Chemical Vapour Deposition (CVD) process. Layers of MoS_2 were grown on Silicon dioxide (Sio_2)/Silicon (Si) substrate. Silver nanowires in ethanol solution were dropcasted onto MoS_2 sample. Silver nanowires were grown in single crystalline form and it had around 3-4 nm of Poly Vinyl Pyrrolidone (PVP) layer on it. The wires resting on few layers of MoS_2 (2 to 3 layers) was selected for experiments (Figure 4.1 b).

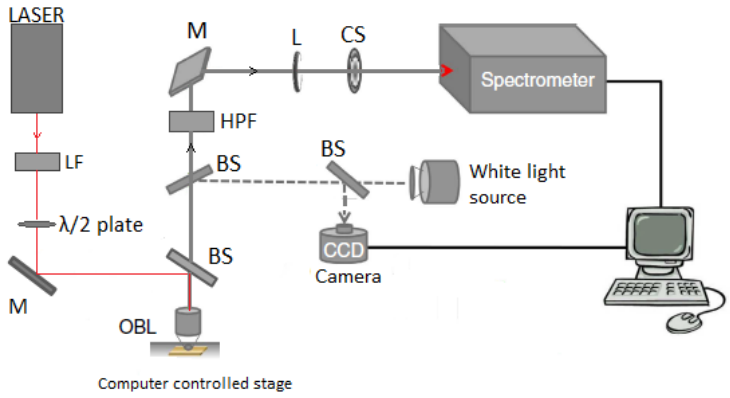

(a)

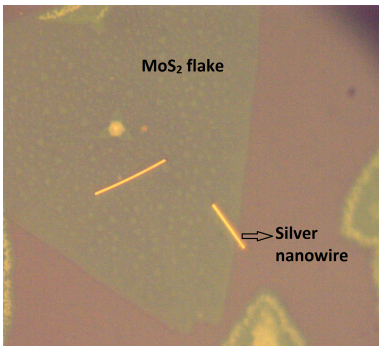

(b)

Figure 4.1: a) Spectroscopy setup for collecting Photoluminescence from silver nanowires on MoS_2 flakes. BS:Beam splitter, M:Mirror, L:Lens, CS:Confocal slit, HPF:High Pass Filter, LF:Line filter(for 633nm laser), OBL:Objective Lens, $\frac{\lambda}{2}$ plate is half wave plate. Excitation was done with 633 nm He-Ne Laser. b)Optical image of Silver nanowire on MoS_2 flake

Centre of nanowire was excited with 633 nm laser and the light was collected from the same point and routed to the spectrometer. Confocal setup was used to collect spectra from a small region on sample plane. The setup is as shown in figure 4.1 a. The collection time of spectra was 10 seconds. Spectra from bare MoS_2 ie area on MoS_2 flake where there were no wires was also collected. Both the spectra were compared.

4.3 Results

The following is the dark field image of a MoS_2 flake from which fluorescence can be seen.

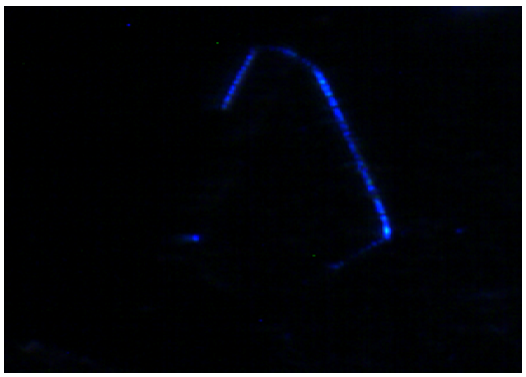

Figure 4.2: Dark field image of MoS_2 flake

Monolayer MoS_2 shows fluorescence from its surface too. But the MoS_2 flake in figure 4.2 is more than one layer and since fluorescence is not so high in few layers and bulk MoS_2 only the edges are fluorescing. We observed enhancement in Photoluminescence in wire on MoS_2 case compared to that on bare MoS_2 in most cases. This is on expected lines and has been already shown previously.

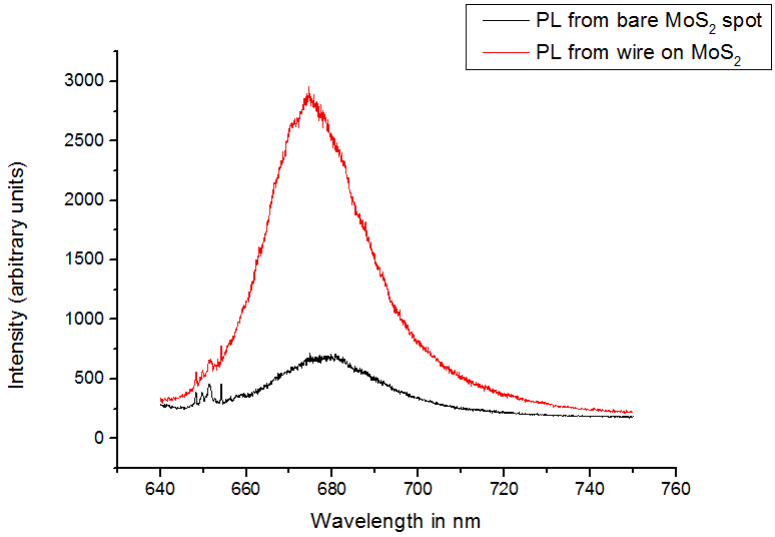

Figure 4.3: Comparison of Photoluminescence from silver nanowire on MoS_2 and bare MoS_2

Photoluminescence peaks at 680 nm for both the cases. Raman peaks can be seen in the range of 650 nm to 660 nm. They are the characteristic peaks of MoS_2. No modification is seen in Raman peaks of MoS_2 due to the presence of wire. The extent to which Photoluminescence is enhanced varied from sample to sample. This is quantified by Enhancement factor (EF). This is given by ratio of area under the curve for wire on MoS_2 to that of bare MoS_2. $EF = \frac{Area_{wire}}{Area_{MoS_2}}$. For the above case, this turns out to be 5.2 .

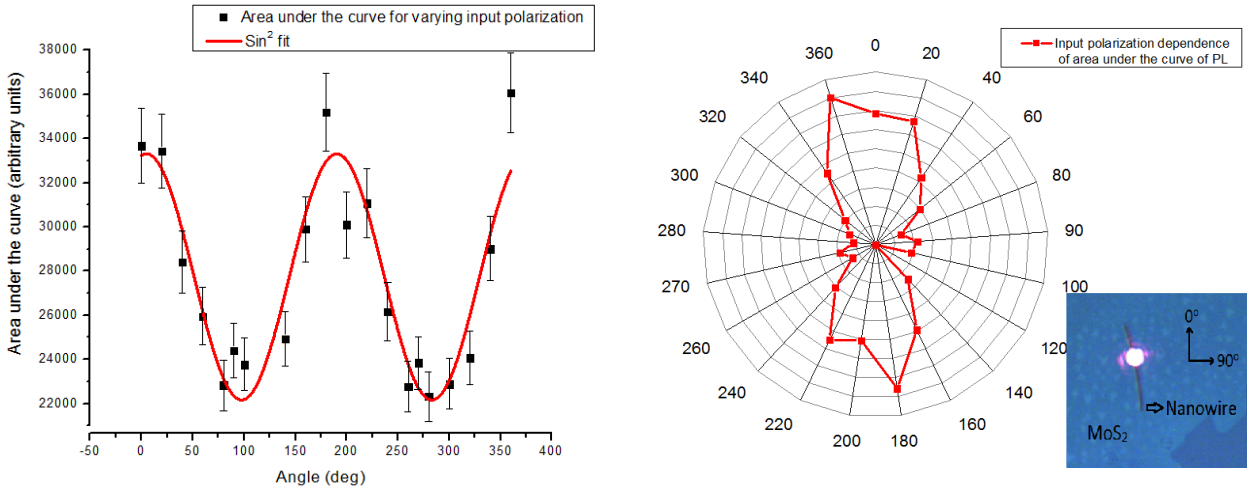

Figure 4.4: Effect of input polarization on Photoluminescence a)Fitting of data with Sin^2 curve b)Polar plot of data points. Inset: Nanowire on MoS_2 flake with the point of excitation is shown. The sense of angle of polarization with respect to the wire is also shown.

We also studied the effect of input polarization on the excitonic emission from wire on MoS_2. A half-wave plate ($\frac{\lambda}{2}$) was inserted in the input path. The angle was varied from 0^o to 180^o in the steps of 5^o. Angle θ in half-wave plate produces a shift of 2θ in the angle of polarization. When the angle of polarization is zero, light is polarized along the wire. Light is polarized perpendicular to the direction of wire when the angle of polarization is 90 degrees. It can be seen from figure 4.4 (a) that maximum photoluminescence is obtained when the light is polarized along the wire and is minimum when angle of polarization is 90^o. The data points are fit to Sin^2 curve. The sinusoidal fitting was a guess. It can be justified by the fact that polarization dependence is generally Sin^2 function. Considering experimental errors it is a good fit with $R^2 = 0.85$. Error bars are plotted which are 5% of the value of intensity of Photoluminescence. Polar plot also shows two- lobe pattern of Sin^2 function.(Fig. 4.4 (b))

4.4 Discussion

Even though in most of the cases we observed an enhancement of photoluminescence, there were also a few cases where there was quenching of emission. This can be explained based on the fact that the PVP layer on nanowires acts as a spacer between metal and MoS_2. The wires which had no PVP layer on them came in direct contact with the semiconductor which resulted in quenching of photoluminescence of MoS_2. the mathematical formalism for the above argument goes as follows.

Upon excitation, excitons are formed in semiconductors. The exciton recombination produces emission. The exciton recombination rate is given by

$\gamma_{tot} = \gamma_{rad} + \gamma^0_{non-rad} + \gamma_{non-rad,metal}$

Here non-radiative recombination due to the presence of metal contributes to quenching and radiative term to the enhancement of emission. γ_{rad} denotes radiative recombination term. $\gamma^0_{non-rad}$ and $\gamma_{non-rad,metal}$ are non-radiative recombination terms for a semiconductor in the absence of metal and in the presence of metal respectively. The quantum yield of emission is given by $Y = \frac{\gamma_{rad}}{\gamma_{tot}}; Y_0 = \frac{\gamma^0_{rad}}{\gamma^0_{tot}}$($Y_0$ - in the absence of metal).

The quantities I_{abs}, I^0_{abs} are the Intensities of light absorption by semiconductor in the presence and absence of metal respectively. $\omega_{laser}(\omega_{ems})$ is the laser excitation(exciton emission) frequency. $I_{abs} = P(\omega_{laser})I^0_{abs}$ and $\gamma_{rad} = P(\omega_{ems})\gamma^0_{rad}$

$P(\omega)$ is the electromagnetic-field enhancement factor.

$P(\omega) = \frac{< |\overline{E}|^2_{metal} >_{\Omega,t}}{< E^2_{nometal} >_t}$ E_{metal} and $E_{nometal}$ are the electric field integrated in the whole volume of semiconductor nanoparticle. Another average is over Ω (solid angle defined for the direction of laser field) and time.

Emission intensity $I_{ems}(\omega_{ems}) = \frac{P(\omega_{ems})\gamma^0_{rad}P(\omega_{laser})I^0_{abs}}{P(\omega_{ems})\gamma^0_{rad} + \gamma^0_{non-rad} + \gamma_{non-rad,metal}(\omega_{ems})}$

The crucial term in this equation is $\gamma_{non-rad,metal}(\omega_{ems}$ which can be found using the well known Fermi's golden rule for spontaneous emission.

$\gamma_{non-rad,metal}(\omega_{ems}) = \frac{2\pi}{\hbar} < \sum_f | < 0_{exc}; f|\hat{V}_{int}|exc; 0_{pl} > |^2 \delta(\hbar\omega_{exc} - \hbar\omega_f) >$

In the above matrix element, $|exc; 0_{pl}>$ denotes initial state in which exciton is in semiconductor nanoparticle and $|0_{exc}; f>$ denote final states where there is plasmon excitation in metal nanoparticle and no exciton in semiconductor nanoparticle. The energies of these states are given by $\hbar\omega_{exc}$ and $\hbar\omega_f$. The Coulombic interaction between carriers in different nanoparticles is given by $\hat{V}_{int}$.

In [24], semiconductor and metal nanoparticles are considered. Hence spherical harmonics is employed to calculate the potential in the nanoparticles. For d(distance between centres of metal and semiconductor particles)>> R_{metal} (Radius of metal particle), R_{sm}(Radius of semiconductor particle), dipole approximation said to be valid. In that case, it has been shown that $\gamma_{non-rad,metal} \propto \frac{1}{d^6}$, that is at large separation. Whereas for when both particles close to each other, $\gamma_{non-rad,metal} \propto \frac{1}{\Delta^4}$, where Δ is the shortest distance between surface of two particles. Hence it has been shown that non-radiative decay due to metal nanoparticle decreases with increasing separation between particles. In [25], it has been shown that quenching efficiency drastically decreases after a certain separation distance. It can be argued that in the competition between non-radiative and radiative decay, radiative decay term dominates for large distances which result in enhancement of excitonic emission. Because of the presence of metal, local density of states changes in Fermi's golden rule expression which results in enhanced spontaneous emission. Another way of looking at this is due to the coupling of excitons and plasmons, the hot electrons generated in metal are transferred to the conduction band of MoS_2 and contributes to the Photoluminescence emission [26]. Even though the above mathematical formalism is for spherical nanoparticles, it can also be extrapolated to the system we are studying.

It is interesting to see that difference in Photoluminescence in parallel and perpendicularly polarized light is not significant when compared to that of bare MoS_2. The polarization dependence of Photoluminescence is quite counter-intuitive result. Perpendicularly polarized light with respect to the wire should have more localization and hence more should be the Photoluminescence. Parallel polarization should have propagation and hence less local field at the point of excitation resulting lesser Photoluminescence when compared to that of perpendicular polarization case. But the results we have obtained are exactly opposite to this. However, polarization studies on the same system have been done by other groups with excitation from one end and collection from the other end [27], and results similar to our have been obtained.

All in all, modulation of excitonic emission of MoS_2 in the presence of silver nanowire has been shown in this chapter. Polarization dependence of Photoluminescence again gives control over the excitonic emission. It can be said that silver nanowire is acting as an antenna if it enhances the emission and directs it to one particular direction. The directionality of emission is discussed in the next chapter.

Chapter 5

Fourier plane study of Silver nanowires on MoS_2 system

5.1 Motivation

It is an important information to know how a plasmonic component scatters light in far field from the point of view of application. It is not just the measurement of the magnitude of scattering cross section but the distribution of scattered light in each direction also matters. The technique to measure the angular radiation pattern in far field is called 'Fourier microscopy' or 'back focal plane imaging'. [28]

As mentioned in the previous chapter, silver nanowires are known to act as nanoantennas [29]. Our aim was to investigate if this characteristic of nanowire also affects the emission of MoS_2. MoS_2 can be modelled as series of in-plane dipoles. As seen in the previous chapter, silver nanowire which is a metal, affects the magnitude of emission of these dipoles. Because of the geometry of wires, it should also affect the directionality of emission of dipoles in its vicinity. According to the spectra, there were both Raman and Photoluminescence signal from Wire on MoS_2 system. One would also be interested in how both of these modes are emitted in Fourier space.

5.2 Fourier plane microscopy

When an object is placed at the focus of a lens, the Fourier transform of the object is produced at the focal plane in the image plane side which is also called 'back focal plane'. In figure 5.1, all parallel rays with same wavevector(k) meet at a point in back focal plane. Hence it is also called k-space or momentum space as the Fourier transform of position should give the information about momentum and it is related to 'k' as $p = \hbar k$. [30]

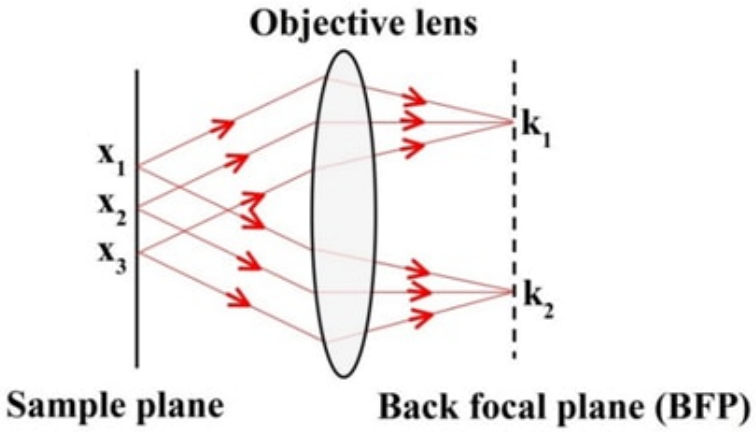

Figure 5.1: Parallel rays meeting at back focal plane

The waves emanating from an object can be seen as the superposition of plane waves. Consider a plane wave of complex amplitude $E(x, y, z) = Aexp[i(k_x x + k_y y + k_z z)]$. Here the wavevector $k = (k_x, k_y, k_z)$. The wavevector makes an angle $\theta_x = sin^{-1}(\frac{k_x}{k})$with y-z plane and $\theta_y = sin^{-1}(\frac{k_y}{k})$ with x-z plane.

The function in $z = 0$ plane, $E(x, y, 0)$ is a spatial harmonic that is a sinusoidal function $F(x, y) = Aexp[2\pi i(v_x x + v_y y)]$ with spatial frequencies $v_x = \frac{k_x}{2\pi}, v_y = \frac{k_y}{2\pi}$. Therefore $\theta_x = sin^{-1}\lambda v_x, \theta_y = sin^{-1}\lambda v_y$ In the paraxial approximation, $\theta_x \approx \lambda v_x, \theta_y \approx \lambda v_y$ Thus the angle of inclination is directly proportional to the spatial frequencies of harmonic function.

As shown in figure 16, a lens focuses each plane wave travelling in the direction (θ_x, θ_y)onto a single point $(\theta_x f, \theta_y f)$in the focal plane. Thus the lens spatially separates the contribution of different harmonic functions. A point in focal plane $x' = \theta_x f = \lambda v_x f, y' = \theta_y f = \lambda v_y f$

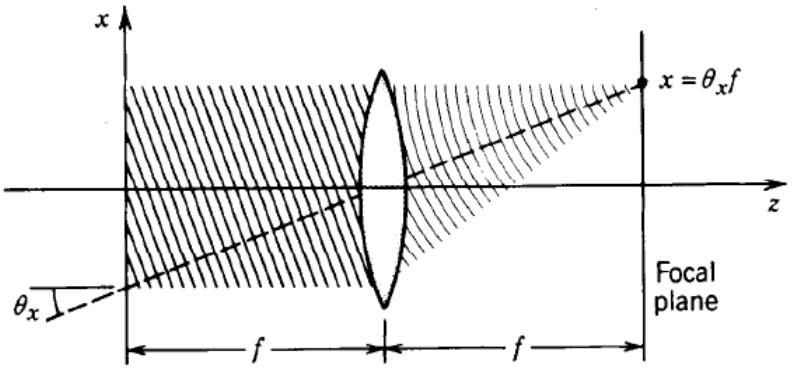

Figure 5.2: Focusing of a plane wave into a point in fourier plane. A direction (θ_x, θ_y) is mapped into (x,y)= $(\theta_x f, \theta_y f)$ at z=2f [6]

. Therefore by above arguments, one can say that the lens Fourier transforms the function F(x,y,z=0) at z=2f namely G(v_x, v_y). And the value of F(x,y,z=2f) at the output, that is at the focal plane is proportional to the Fourier transform of F(x,y,z=0).

$$F(x, y, z = 2f) \propto G(x', y') \text{ [6]}$$

In 2-dimensions, the different co-ordinates in the back focal plane image is as shown in figure 5.3.

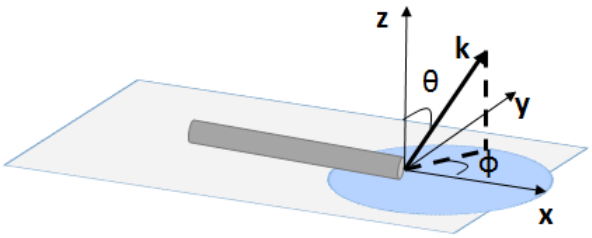

Figure 5.3: The definition of θ and ϕ co-ordinates in back focal plane

5.3 Setup

Back focal plane imaging is generally realized using a high numerical aperture objective lens. The back aperture of the objective lens contains the k-space information of the emitted light

from the sample. It is not possible to capture an image from this plane directly as this plane is formed between objective and eyepiece. Hence the back focal plane is relayed to conjugate back focal plane as shown in Figure 5.4 [31] [32]

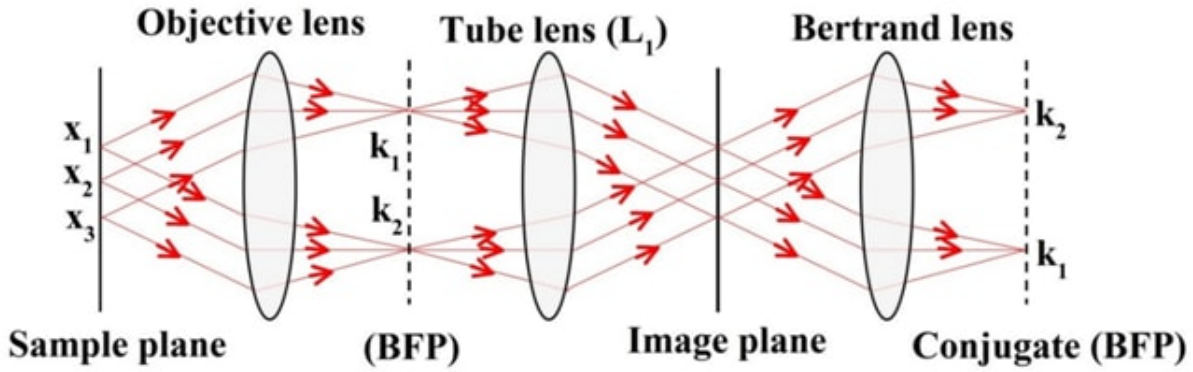

Figure 5.4: Realization of back focal plane imaging using Tube lens and Bertrand lens

Here the tube lens is placed such that its distance from the back focal plane is equal to its focal length. It produces a real plane image at its focal point. Bertrand lens is placed such that its distance from the image plane of tube lens is equal to its focal length. Hence the back focal plane is again reproduced at conjugate back focal plane. The magnification of this image is dependent on the focal lengths of tube lens and Bertrand lens.

Based on this principle, a Fourier plane imaging setup was already built in our lab. The diagram of which is shown in figure 5.5. All our studies have been done with 633 nm Helium-Neon laser. The back focal image is captured in the Electron Multiplying Charged Coupled Device (EMCCD) which is a highly sensitive CCD. The spectra of the back focal images can also be captured by this setup which is called energy-momentum (E-k) spectroscopy. Here L1 acts as tube lens and L2 as Bertrand lens. L3 is flip lens; when it is inserted, real plane images instead of back focal plane images are captured.

Our system comprising of silver nanowires resting on few layers of MoS_2 was studied by this technique.

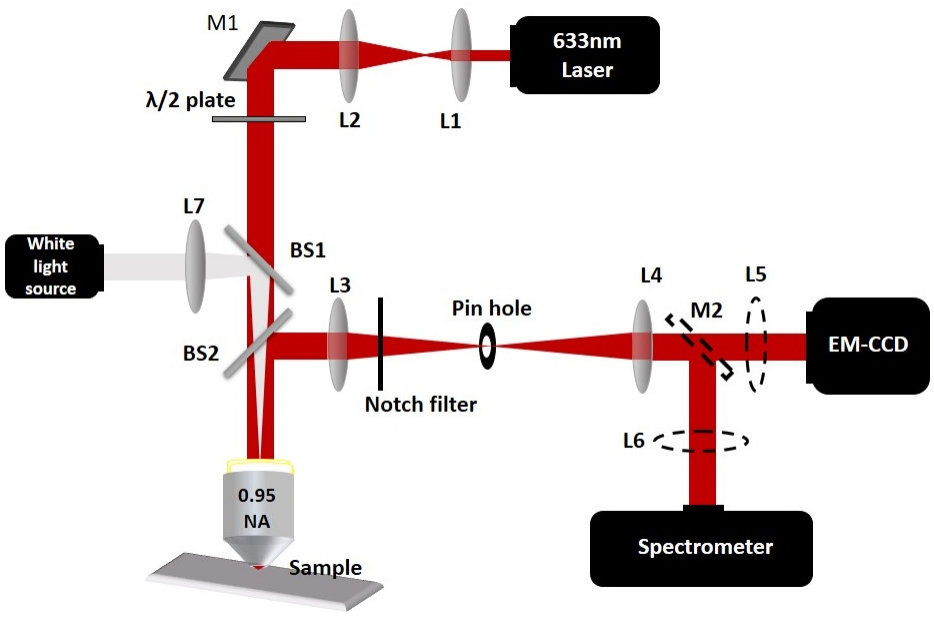

Figure 5.5: Fourier plane imaging and spectroscopy setup. BS:Beam Splitters, M1,M2:Mirrors, L1 to L7: Biconvex lenses, $\frac{\lambda}{2}$ plate:Half wave plate

5.4 Results

By observing the sample using a white light source, those MoS_2 flakes were identified on which nanowire is fully overlapping on it. Spectra was taken from bare MoS_2 part. If the Photoluminescence counts were high when compared to Raman peak intensity, such flakes were chosen as they were convenient to take back focal plane images. Objective lens of 0.95 NA was used for the experiment. After the L1 lens, Edge filter was placed so as to cut down the light due to Rayleigh scattering that is 633nm light. Similar to the experiment in the previous chapter, a wire was illuminated by the laser at the center of it as shown in 19 (c). The back focal images for one such sample is shown in Figure 5.6 (a) and (b).

As a convention, x-axis is chosen to be along the direction of wire and y-axis to be perpendicular to it. Corresponding to it, k_x and k_y can be interpreted. In the back focal plane images, $\theta_{max} = 0.95$ is the limit. This is the maximum angle of radiation that can be captured as the numerical aperture of the objective lens is 0.95.

Back focal plane image in 5.6(a) of the emission of bare MoS_2 is a uniform blob with

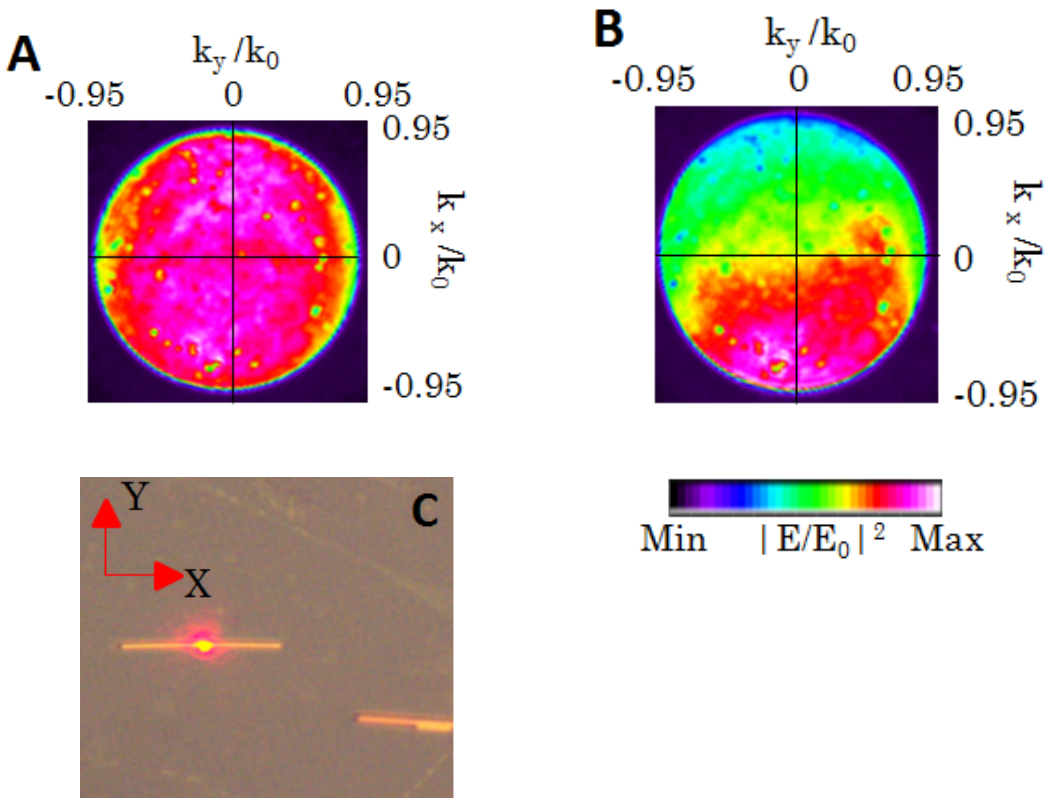

Figure 5.6: Back focal plane (BFP)images of emission from A)Bare MoS_2 B)Silver nanowire on MoS_2 C)Optical image of the silver nanowire on MoS_2 from which the BFP image was taken. Scale bar for the intensity of back focal plane images

intensity symmetrical in all θs and ϕs. But in the case of wire on MoS_2, the emission favours only one direction perpendicular to the wire and occupies a relatively small region in k-space. Hence we observe nano-antenna effect as anticipated.

5.5 Discussion

Layered MoS_2 is to be an array of inplane dipoles. The direct bandgap transition and indirect bandgap transition from MoS_2 is shown to be inplane oriented by energy and momentum resolved spectroscopy [33]. The emission from in-plane dipoles when collected from air side should show up as a uniform blob in the back focal plane [34].

Figure 5.7 shows the emission pattern of a dipole oriented along x-axis which is a in-plane

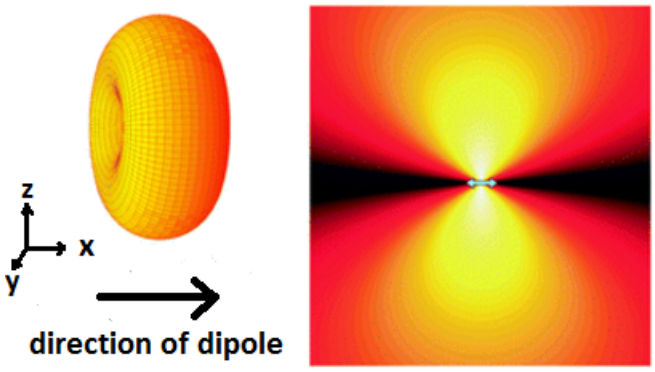

Figure 5.7: Doughnut-shaped emission of a dipole oriented along x-axis [7]

case in our experiment. X-Y plane is our sample plane hence it is the in-plane in our case. When viewed from z-axis from the top, one should see uniform emission in all directions [35]. MoS_2 being an array of in-plane dipoles shows this behaviour experimentally. Hence this well known is verified in figure 5.6(a).

In the case of wire on MoS_2 (Fig. 5.6(b)), this excitonic emission is modified and is directed to one region in k-space. This result is yet to be explained by us. One surprising fact is that the emission is in one perpendicular direction to wire and this direction could have been any of the perpendicular directions. When there is no apparent asymmetry in these directions why is one of them preferred is to be answered. One might think that this is because of scattering due to the surface of nanowires. But this is not the case, as even if we move the excitation spot slightly along the width of wire, the emission pattern doesn't change significantly. Also if it was just surface scattering, the emission would have been just Rayleigh light. But since we are using Edge/Notch filters, majority of Rayleigh light(633nm in our case) is blocked.

One way to answer these questions is to model our system. Modelling MoS_2 is not very straightforward. We made an attempt to model it in COMSOL by thinking of it as an array of dipoles [33]. But there are a lot of arbitrary parameters in that case such as the distance between the dipoles, arrangement of dipoles with respect to wires etc. Also, this did not give any satisfactory and consistent results.

5.6 Future directions

The complex dielectric function of MoS_2 has been modelled as a superposition of Lorentzian oscillators [36]. This can be employed in our studies. The complex dielectric function, $\epsilon(E) = \epsilon_1(E) + i\epsilon_2(E)$ as a function of incident photon energy E is given by a superposition of Lorentzian oscillators.

$$\epsilon(E) = 1 + \sum_{k=1}^{N} \frac{f_k}{E_k^2 - E^2 - iE\gamma_k}$$

f_k is the oscillator strength and γ_k line width of k^{th} oscillator. The interval of E_k can be chosen according to the convenience. Monolayer MoS_2 can be thought of as a layer of thickness d=6.15 Å [37] which is the interlayer spacing of MoS_2 with the above dielectric function. This can be realized in COMSOL software.

We can also study propagating modes of silver wire on MoS_2. As such light propagation was not observed in wires in our system. By coating MoS_2 sample with a SiO_2 spacer and then dropcasting wire, propagation can be achieved [38]. An advantage with studying propagated light in the Fourier plane is that the scattering due to the surface of nanowires is eliminated. Also how different modes of MoS_2 are propagating can also be studied by doing Energy-Momentum spectroscopy (E-k) on the back focal plane images we obtain [39]. This will have implications in nanophotonic circuits.

Bibliography

[1] Rashid Zia, Jon A. Schuller, Anu Chandran, and Mark L. Brongersma. Plasmonics: the next chip-scale technology. *Materials Today*, 9(78):20 – 27, 2006.

[2] Qing Hua Wang, Kourosh Kalantar-Zadeh, Andras Kis, Jonathan N Coleman, and Michael S Strano. Electronics and optoelectronics of two-dimensional transition metal dichalcogenides. *Nature nanotechnology*, 7(11):699–712, 2012.

[3] Branimir Radisavljevic, Aleksandra Radenovic, Jacopo Brivio, i V Giacometti, and A Kis. Single-layer mos2 transistors. *Nature nanotechnology*, 6(3):147–150, 2011.

[4] Intek Song, Chibeom Park, and Hee Cheul Choi. Synthesis and properties of molybdenum disulphide: from bulk to atomic layers. *RSC Adv.*, 5:7495–7514, 2015.

[5] Roushdey Salh. *Defect related luminescence in silicon dioxide network: a review*. INTECH Open Access Publisher, 2011.

[6] B.E.A. Saleh and M.C. Teich. *Fundamentals of Photonics*. Wiley Series in Pure and Applied Optics. Wiley, 2007.

[7] Dominik Woll, Els Braeken, Ania Deres, Frans C. De Schryver, Hiroshi Uji-i, and Johan Hofkens. Polymers and single molecule fluorescence spectroscopy, what can we learn? *Chem. Soc. Rev.*, 38:313–328, 2009.

[8] Kathryn M. Mayer and Jason H. Hafner. Localized surface plasmon resonance sensors. *Chemical Reviews*, 111(6):3828–3857, 2011. PMID: 21648956.

[9] Jana Olson, Sergio Dominguez-Medina, Anneli Hoggard, Lin-Yung Wang, Wei-Shun Chang, and Stephan Link. Optical characterization of single plasmonic nanoparticles. *Chem. Soc. Rev.*, 44:40–57, 2015.

[10] Liane Slaughter, Wei-Shun Chang, and Stephan Link. Characterizing plasmons in nanoparticles and their assemblies with single particle spectroscopy. *The Journal of Physical Chemistry Letters*, 2(16):2015–2023, 2011.

[11] Xiao Xu, Tian Li, Zhongxing Xu, Hejia Wei, Ruoyun Lin, Bin Xia, Feng Liu, and Na Li. Automatic enumeration of gold nanomaterials at the single-particle level. *Analytical chemistry*, 87(5):2576–2581, 2015.

[12] Andrea Splendiani, Liang Sun, Yuanbo Zhang, Tianshu Li, Jonghwan Kim, Chi-Yung Chim, Giulia Galli, and Feng Wang. Emerging photoluminescence in monolayer mos2. *Nano letters*, 10(4):1271–1275, 2010.

[13] Kin Fai Mak, Keliang He, Changgu Lee, Gwan Hyoung Lee, James Hone, Tony F Heinz, and Jie Shan. Tightly bound trions in monolayer mos2. *Nature materials*, 12(3):207–211, 2013.

[14] Kin Fai Mak, Changgu Lee, James Hone, Jie Shan, and Tony F Heinz. Atomically thin mos 2: a new direct-gap semiconductor. *Physical Review Letters*, 105(13):136805, 2010.

[15] Kartik N Shinde, SJ Dhoble, HC Swart, and Kyeongsoon Park. Introduction. In *Phosphate Phosphors for Solid-State Lighting*, pages 1–39. Springer, 2012.

[16] Justin L. Burt, Jose L. Elechiguerra, Jose Reyes-Gasga, J. Martin Montejano-Carrizales, and Miguel Jose-Yacaman. Beyond archimedean solids: Star polyhedral gold nanocrystals. *Journal of Crystal Growth*, 285(4):681 – 691, 2005.

[17] Wenxin Niu, Yi An Alvin Chua, Weiqing Zhang, Hejin Huang, and Xianmao Lu. Highly symmetric gold nanostars: crystallographic control and surface-enhanced raman scattering property. *Journal of the American Chemical Society*, 137(33):10460–10463, 2015.

[18] David J Hill, Christopher W Pinion, Joseph D Christesen, and James F Cahoon. Waveguide scattering microscopy for dark-field imaging and spectroscopy of photonic nanostructures. *Acs Photonics*, 1(8):725–731, 2014.

[19] P Zijlstra and M Orrit. Single metal nanoparticles: optical detection, spectroscopy and applications. *Reports on Progress in Physics*, 74(10):106401, 2011.

[20] Kevin CJ Lee, Yi-Huan Chen, Hsiang-Yu Lin, Chia-Chin Cheng, Pei-Ying Chen, Ting-Yi Wu, Min-Hsiung Shih, Kung-Hwa Wei, Lain-Jong Li, and Chien-Wen Chang. Plasmonic gold nanorods coverage influence on enhancement of the photoluminescence of two-dimensional mos2 monolayer. *Scientific reports*, 5:16374, 2015.

[21] Alejandro Molina-Sánchez, Kerstin Hummer, and Ludger Wirtz. Vibrational and optical properties of mos 2: From monolayer to bulk. *Surface Science Reports*, 70(4):554–586, 2015.

[22] Zhipeng Li, Feng Hao, Yingzhou Huang, Yurui Fang, Peter Nordlander, and Hongxing Xu. Directional light emission from propagating surface plasmons of silver nanowires. *Nano letters*, 9(12):4383–4386, 2009.

[23] Hyun Seok Lee, Dinh Hoa Luong, Min Su Kim, Youngjo Jin, Hyun Kim, Seokjoon Yun, and Young Hee Lee. Reconfigurable exciton-plasmon interconversion for nanophotonic circuits. *Nature Communications*, 7:13663 EP –, Nov 2016. Article.

[24] Alexander O Govorov, Garnett W Bryant, Wei Zhang, Timur Skeini, Jaebeom Lee, Nicholas A Kotov, Joseph M Slocik, and Rajesh R Naik. Exciton- plasmon interaction and hybrid excitons in semiconductor- metal nanoparticle assemblies. *Nano letters*, 6(5):984–994, 2006.

[25] Zoher Gueroui and Albert Libchaber. Single-molecule measurements of gold-quenched quantum dots. *Phys. Rev. Lett.*, 93:166108, Oct 2004.

[26] Ziwei Li, Yingdong Xiao, Yongji Gong, Zongpeng Wang, Yimin Kang, Shuai Zu, Pulickel M Ajayan, Peter Nordlander, and Zheyu Fang. Active light control of the mos2 monolayer exciton binding energy. *ACS nano*, 9(10):10158–10164, 2015.

[27] Kenneth M Goodfellow, Ryan Beams, Chitraleema Chakraborty, Lukas Novotny, and Anthony N Vamivakas. Integrated nanophotonics based on nanowire plasmons and atomically thin material. *Optica*, 1(3):149–152, 2014.

[28] Ivana Sersic, Christelle Tuambilangana, and A Femius Koenderink. Fourier microscopy of single plasmonic scatterers. *New Journal of Physics*, 13(8):083019, 2011.

[29] Timur Shegai, Vladimir D Miljkovic, Kui Bao, Hongxing Xu, Peter Nordlander, Peter Johansson, and Mikael Kall. Unidirectional broadband light emission from supported plasmonic nanowires. *Nano letters*, 11(2):706–711, 2011.

[30] E. Hecht. *Optics*. Addison-Wesley, 2002.

[31] Jonathan A Kurvits, Mingming Jiang, and Rashid Zia. Comparative analysis of imaging configurations and objectives for fourier microscopy. *JOSA A*, 32(11):2082–2092, 2015.

[32] Arindam Dasgupta, Danveer Singh, Ravi P. N. Tripathi, and G. V. Pavan Kumar. Directional fluorescence emission mediated by chemically-prepared plasmonic nanowire junctions. *The Journal of Physical Chemistry C*, 120(31):17692–17698, 2016.

[33] Jon A Schuller, Sinan Karaveli, Theanne Schiros, Keliang He, Shyuan Yang, Ioannis Kymissis, Jie Shan, and Rashid Zia. Orientation of luminescent excitons in layered nanomaterials. *Nature nanotechnology*, 8(4):271–276, 2013.

[34] M Andreas Lieb, James M Zavislan, and Lukas Novotny. Single-molecule orientations determined by direct emission pattern imaging. *JOSA B*, 21(6):1210–1215, 2004.

[35] Lukas Novotny and Bert Hecht. Principles of nano-optics, 2012.

[36] Yilei Li, Alexey Chernikov, Xian Zhang, Albert Rigosi, Heather M Hill, Arend M van der Zande, Daniel A Chenet, En-Min Shih, James Hone, and Tony F Heinz. Measurement of the optical dielectric function of monolayer transition-metal dichalcogenides: Mos 2, mo s e 2, ws 2, and ws e 2. *Physical Review B*, 90(20):205422, 2014.

[37] Ryan J. Wu, Michael L. Odlyzko, and K. Andre Mkhoyan. Determining the thickness of atomically thin mos2 and {WS2} in the {TEM}. *Ultramicroscopy*, 147:8 – 20, 2014.

[38] Hyun Seok Lee, Min Su Kim, Youngjo Jin, Gang Hee Han, Young Hee Lee, and Jeongyong Kim. Selective amplification of the primary exciton in a mo s 2 monolayer. *Physical review letters*, 115(22):226801, 2015.

[39] Tim H Taminiau, Sinan Karaveli, Niek F Van Hulst, and Rashid Zia. Quantifying the magnetic nature of light emission. *Nature communications*, 3:979, 2012.

[40] J M Pitarke, V M Silkin, E V Chulkov, and P M Echenique. Theory of surface plasmons and surface-plasmon polaritons. *Reports on Progress in Physics*, 70(1):1, 2007.

Appendix

A classical approach to surface plasmon polariton

Surface Plasmon condition: We consider two media with dielectric function ϵ_1 and ϵ_2 separated by z=0. In the absence of external sources, Maxwell's equations can be written as,

$$\nabla X H_i = \epsilon_i \frac{1}{c} \frac{\partial}{\partial t} E_i$$

$$\nabla X E_i = -\frac{1}{c} \frac{\partial}{\partial t} H_i$$

$$\nabla.(\epsilon_i E_i) = 0, \qquad \nabla.H_i = 0$$

where i denotes variables in different media, i=1 at $z < 0$ (metal medium) and i=2 at $z > 0$ (dielectric medium). Given the condition that waves are propagating, there has to be a component of electric field normal to the interface. As a consequence of this, magnetic field should be parallel to the surface. Choosing x-axis to be the direction of propagation.

$$E_i = (E_{i_x}, 0, E_{i_z}) e^{-k|z|} e^{i(q_i x - \omega t)}$$

$$H_i = (0, H_{i_y}, 0) e^{-k|z|} e^{i(q_i x - \omega t)}$$

Substituting these equations into Maxwell's equations, the following conditions are obtained

$$ik_1 H_{1_y} = \frac{\omega}{c}\epsilon_1 E_{1_x}$$

$$ik_1 H_{2_y} = -\frac{\omega}{c}\epsilon_2 E_{2_x} \text{ and}$$

$$k_i = \sqrt{q_i^2 - \epsilon_i \frac{\omega^2}{c^2}}$$

Applying boundary conditions, all parallel components to the surface must be equal. We get following conditions.

$$H_{1_y} - H_{2_y} = 0$$

$$\frac{k_1}{\epsilon_1} H_{1_y} + \frac{k_2}{\epsilon_2} H_{2_y} = 0$$

This set of equations has solutions if the determinant is zero. This gives

$$\frac{\epsilon_1}{k_1} + \frac{\epsilon_2}{k_2} = 0$$

This is the surface plasmon condition. [40]

Applying the continuity condition to q, we get $q_1 = q_2 = q$. Hence the surface plasmon condition can also be written as

$$q(\omega) = \frac{\omega}{c}\sqrt{\frac{\epsilon_1 \epsilon_2}{\epsilon_1 + \epsilon_2}}$$